Research Article

Journal of Oil and Gas Research Reviews

Heat Generation/Absorption Effect on Mixed Convection Flow in A Vertical Channel Filled with A Nanofluid: Exact Solution

Michael O. Oni* and Basant K. Jha

Department of Mathematics, Ahmadu Bello University, Zaria, Nigeria.

***Corresponding Author**
Michael O. Oni, Department of Mathematics, Ahmadu Bello University, Zaria, Nigeria.

Submitted: 27 Oct 2022; **Accepted:** 20 Dec 2022; **Published:** 24 Jan 2023

Citation: Oni, M.O. & Jha, B.K. (2023), Heat Generation/Absorption Effect on Mixed Convection Flow in A Vertical Channel Filled with A Nanofluid: Exact solution, *Journal of Oil and Gas Research Reviews*. 3(1), 01-14.

Abstract

An exact solution to discuss the role of heat source/sink on mixed convection flow in a vertical channel filled with nanofluid is presented in this article. The governing momentum, energy and concentration equations are presented and the effects of Brownian's motion, thermophoresis as well as buoyancy-ratio distributions are accounted for. Using the constant heat source/sink (CHSS) and temperature dependent heat source/sink mathematical models (TDHSS), exact solutions are obtained for dimensionless temperature, nanoparticle volume fraction, velocity, Nusselt number, Sherwood number as well as skin-friction. It is established that CHSS case transfers more heat compared to the TDHSS.

Relevance of the work

In this article, theoretical investigation on role of various forms of heat source on flow formation and heat transfer of mixed convection flow is extensively discussed. The findings in this article have significant application in cooling of micro-electronic equipment devices and heat sink.

Keywords: Nanofluid; Heat Source/Sink; Exact Solution; Vertical Channel.

Nomenclature

c	heat capacity at constant pressure
C	nanoparticles volume fraction
D_B	Brownian diffusion coefficient
D_T	thermophoretic diffusion coefficient
g	acceleration due to gravity
Gr	Grashof number
h	distance between parallel walls
Nb	Brownian motion parameter
Nr	buoyancy-ratio parameter
Nt	thermophoresis motion parameter
Nu	Nusselt number
p	pressure
Q_0	dimensional heat source/sink parameter
Re	Reynolds number
S	dimensionless heat source/sink parameter for TDHSS
S_0	dimensionless heat source/sink parameter for CHSS
Sh	Sherwood number
T	dimensional temperature
$\mathbf{V}$	dimensional velocity vector
u, v	velocity components in the and directions respectively
U	dimensionless velocity
x, y	Cartesian coordinates
X, Y	dimensionless Cartesian coordinates

Greek Symbols

β	thermal expansion coefficient
ϕ	rescaled nanoparticle volume fraction
κ	thermal conductivity
μ	dynamic viscosity
ν	kinematic viscosity
θ	dimensionless temperature
ρ	density

Subscripts

f	fluid
p	solid particle

Introduction

The applications of heat and mass transfer in recent engineering and scientific devices cannot be over emphasized. These applications include collection of solar energy, cooling devices in electronics and micro-electronic equipment's, heat sink, nuclear waste disposal, exothermic reactions in catalytic beds and underground spreading of chemical wastes and pollutants. A review of related literatures show that different articles have been devoted to understanding heat and mass transfer of mixed convection flow in different geometries. The earliest studies include the work of Tao, Aung and Work and Lavine where they studied the fully developed forced and natural convection flow

in vertical channel [1-3].

Over the years, it has been established that the conventional heat transfer fluids (water, oil) are poor heat transfer fluids, due to their small thermal conductivity. To overcome this challenge, researchers have tried to suspend nanoparticles of metals, oxides, carbides to increase the thermal conductivity of the fluid [4]. Theses fluids containing the nanometre sized particles are called nanofluid [5, 6]. It has been established that these nanofluids have superior properties and applications in term of heat and mass transfer, engine cooling/vehicle thermal management, heat exchanger, nuclear cooling and solar collections compared to the conventional fluids. Buongiorno developed a mathematical model to examine the convective transport in nanofluids and noted that the nanoparticle absolute velocity can be viewed as the sum of the base fluid velocity and the slip velocity [7]. Nield and Kuznetzov used the model proposed by to investigate the natural convective boundary-layer flow in a porous medium saturated by a nanofluid. Later, Grosan and Pop also employed the model developed by to study the fully developed mixed convection in a vertical channel filled by a nanofluid [8-11]. They found that Nusselt number is a decreasing function of Brownian motion parameter as well as thermophoresis parameter. It is worth mentioning that the model presented by permits a simple analytical solution [12]. In view of this, several articles with different physical situations have been credited to this phenomenon [13-17].

In attempt to understand the role of heat source/sink on flow formation, Inman and Ostrach, assumed the internal heat generation/absorption to be constant, but considered as a function of space by Chambre and Toor [18-21]. Later, the notion of temperature dependent heat source was introduced by Moalem and Foraboschi and Federico in their works, they presented the volumetric rate of heat generation which is directly proportional to and explained that it approximates the state of some exothermic process with as the ambient temperature [22, 23].

In has been proven that there is occurrence of flow reversal at the channel walls in study of mixed convection flow, and this could be attributed to the mixed convection parameter in the flow formation equation [24-27]. It is of great engineering importance to know the range for which this reverse flow occurs. Aung and Work established the condition for occurrence of flow reversal for fully developed mixed convection flow in a vertical channel. Recently, Oni and Jha et al. investigated the fully developed mixed convection flow in vertical annulus and micro-annulus respectively, and they presented the critical values of mixed convection parameter and established the interval for no-reverse-flow [28-30].

Motivated by the applications of nanofluids in engineering devices, this article is devoted to investigating the effects of heat source/sink on fully developed mixed convection flow formation in a vertical channel filled with nanofluid. Using two different mathematical models (CHSS and TDHSS) for heat source/sink, the governing momentum, energy and concentration equations are obtained and solved exactly in section 2 while results and discussion follow in section 3.

Mathematical Analysis

Consider an incompressible, fully developed, steady, heat generating/absorbing nanofluid in a vertical channel driven by combined buoyancy and constant pressure gradient along the direction of flow. The channel is of width h and the no-slip condition is applied on fluid velocity since the considered analysis is in macro-channel. The temperature and nanoparticle concentration at the wall y=0 are assumed to be T_1 and C_1, while the wall y=h is assumed to have temperature and nanoparticle concentration T_2 and C_2 respectively greater than the wall y=0 as shown in Fig. 1. This temperature difference results to density difference at the walls which setups natural convection in the vertical channel. Also, a constant pressure gradient dp/dx is applied in the direction parallel to flow direction. In addition, the fluid considered is either heat generating (source) or absorbing (sink) fluid. Following all the assumptions above and using the Oberbeck-Boussinesq approximation, the following equations govern the conservation of total mass, momentum, thermal energy and nanoparticle concentration in vectorial form (Ref. [9]):

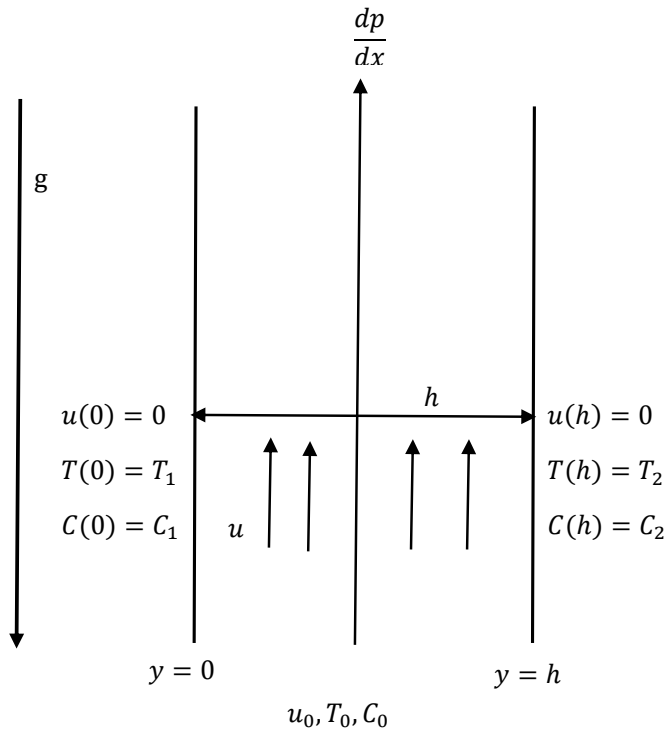

Figure 1: Schematic of the problem

$$\nabla \cdot \mathrm{v} = 0 \tag{1}$$

$$\rho_f(\mathrm{v} \cdot \nabla \mathrm{v}) = -\nabla p + \mu \nabla^2 \mathrm{v} + \{C\rho_p + (1 - C) \times [\rho_f(1 - \beta(T - T_0))]\}\mathrm{g} \tag{2}$$

$$(\rho c)_f(\mathrm{v} \cdot \nabla T) = \kappa \nabla^2 T + (\rho c)_p [D_B \nabla T \cdot \nabla C + (D_T/T_0)\nabla T \cdot \nabla T] + \varphi + Q \tag{3}$$

$$\mathrm{v} \cdot \nabla \mathrm{C} = \mathrm{D}_B \nabla^2 C + (D_T/T_0)\nabla^2 T \tag{4}$$

where C_0 and T_0 are the reference nanoparticle volume fraction concentration and temperature respectively, ρ_p is the nanoparticle mass density, P_f is the fluid density, $(PC)_f$ is the heat capacity of the fluid, $(PC)_p$ is the effective heat capacity of the nanoparticle material and is the dissipation function and is the heat source/sink parameter.

Many mathematical models have been presented to capture heat generation or absorption effect on flow formation in different geometries. We shall consider two cases of these models: constant heat source/sink and the temperature dependent heat source/sink.

Case I: Constant heat source or sink (CHSS)

In the case a uniform heat source/sink is assume throughout the fluid formation and is independent on temperature increase or decrease [31, 32]. Incorporating the fully developed assumption (far from channel's entrance region) on equations (2-4) implies:

$$v = 0, \quad \frac{\partial u}{\partial x} = 0, \quad \frac{\partial T}{\partial x} = 0, \quad \frac{\partial C}{\partial x} = 0, \quad \frac{\partial p}{\partial y} = 0, \quad \frac{\partial p}{\partial x} = \frac{dp}{dx} = \text{constant} \tag{5}$$

Thus, equations (2-4) in dimensional form respectively become:

$$\mu \frac{d^2u}{dy^2} + \{\rho_{f_0}\beta(1 - C_0)(T - T_0) - (\rho_f - \rho_{f_0})(C - C_0)\}\mathrm{g} = \frac{dp}{dx} \tag{6}$$

$$\kappa \frac{d^2T}{dy^2} + (\rho c)_p \left[D_B \frac{dC}{dy}\frac{dT}{dy} + \left(\frac{D_T}{T_0}\right)\left(\frac{dT}{dy}\right)^2\right] + Q_0 = 0 \tag{7}$$

$$D_B \frac{d^2C}{dy^2} + \left(\frac{D_T}{T_0}\right)\frac{d^2T}{dy^2} = 0 \tag{8}$$

Subject to the following boundary conditions

$$u = 0, \qquad T = T_1, \qquad C = C_1, \qquad \text{at} \quad y = 0$$

$$u = 0, \qquad T = T_2, \qquad C = C_2, \qquad \text{at} \quad y = h \tag{9}$$

For fully developed flow, it is usual to assume that the mass flow rate equals to the mass flux throughout the region. Hence, the constant pressure gradient is obtained from:

$$\int_0^h u(y)dy = \int_0^h dy \tag{10}$$

where Q_0 is the dimensional constant heat source/sink parameter?

The following dimensionless parameters, are introduced to transform equations (6-10) into their corresponding dimensionless form:

$$Y = \frac{y}{h}\ ,\ X = \frac{x}{h}\ , U = \frac{u}{u_0}\ ,\ P = \frac{p}{\rho u_0^2}\ ,\ \theta = \frac{(T-T_0)}{T_2-T_0}\ ,\ \phi = \frac{(C-C_0)}{C_2-C_0}\ ,\ T_0 = \frac{(T_1+T_2)}{2}\ ,\ C_0 =$$

$$\frac{(C_1+C_2)}{2},\ Gr = \frac{(1-C_0)g\beta(T_2-T_0)h^3}{\nu^2}\ ,\ Re = \frac{u_0 h}{\nu}\ ,\ Nr = \frac{g(\rho_f-\rho_{f_0})(C_2-C_0)h^2}{\mu u_0}\ ,\ Nb =$$

$$\frac{D_B(C_2-C_0)(\rho c)_p}{\kappa}\ ,\ Nt = \frac{D_B(T_2-C_0)(\rho c)_p}{\kappa T_0}\ ,\ S_0 = \frac{Q_0 h^2(\rho c)_p}{\kappa(T_2-T_1)},\quad S = \frac{Q_0 h^2(\rho c)_p}{\kappa} \tag{11}$$

$$\frac{d^2U}{dY^2} = -\frac{dP}{dX} + Nr\phi - \frac{Gr}{Re}\theta \tag{12}$$

$$\frac{d^2\theta}{dY^2} + Nb\frac{d\theta}{dY}\frac{d\phi}{dY} + Nt\left(\frac{d\theta}{dY}\right)^2 + S_0 = 0 \tag{13}$$

$$\frac{d^2\phi}{dY^2} + \frac{Nt}{Nb}\frac{d^2\theta}{dY^2} = 0 \tag{14}$$

The dimensionless parameter S_0 captures the constant heat source/sink effect. It is good to state that positive values of S_0 signifies heat source (generation) while negative values signifies heat sink (absorption).

$$U = 0, \qquad \theta = -1, \qquad \phi = -1, \qquad \text{at}\ \ Y = 0$$

$$U = 0, \qquad \theta = 1, \qquad \phi = 1, \qquad \text{at}\ \ Y = 1 \tag{15}$$

$$\int_0^1 U(y)dY = 1 \tag{16}$$

Exact solutions to the coupled non-linear equations (10-15) give the dimensionless velocity, temperature and nanoparticle concentration respectively as:

$$U(Y) = -\frac{dP}{dX}\frac{Y^2}{2} + Nr\left[\frac{C_1Y^3}{6} + \frac{C_2Y^2}{2}\right] - \left[\frac{NrNt}{Nb} + \frac{Gr}{Re}\right]\left[\frac{Y^2(S_0+C_3NbC_1)}{2(NbC_1)^2} - \frac{S_0Y^3}{6NbC_1} + \frac{C_4\exp(-NbC_1Y)}{(NbC_1)^2}\right] +$$

$$C_5Y + C_6 \tag{17}$$

$$\theta(Y) = \frac{C_3}{NbC_1} + C_4\exp(-NbC_1Y) - \left[\frac{Y}{NbC_1} - \frac{1}{(NbC_1)^2}\right]S_0 \tag{18}$$

$$\phi(Y) = (2Y-1)\left[1 + \frac{Nt}{Nb}\right] - \frac{Nt}{Nb}\theta(Y) \tag{19}$$

$$\frac{dP}{dX} = E_9 + E_{10}\frac{Gr}{Re} \tag{20}$$

The physical quantities of interest are the skin-friction (τ), Nusselt number$(Nu)$and Sherwood number$(Sh)$and is defined in dimensionless form as:

$$\tau = \left.\frac{dU}{dY}\right|_{Y=0,1}, \qquad Nu = \left.\frac{d\theta}{dY}\right|_{Y=0,1}\ , \qquad \mathrm{Sh} = \left.\frac{d\phi}{dY}\right|_{Y=0,1} \tag{21}$$

$$\tau_0 = \left[\frac{NrNt}{Nb} + \frac{Gr}{Re}\right]\frac{C_4}{NbC_1} + C_5 \tag{22}$$

$$\tau_1 = -\frac{dP}{dX} + Nr\left[\frac{C_1}{2} + C_2\right] - \left[\frac{NrNt}{Nb} + \frac{Gr}{Re}\right]\left[\frac{(S_0 + C_3 NbC_1)}{(NbC_1)^2} - \frac{S_0}{2NbC_1} - \frac{C_4 \exp(-NbC_1)}{NbC_1}\right] + C_5$$

(23)

$$Nu_0 = -C_4 NbC_1 - \frac{S_0}{NbC_1} \tag{24}$$

$$Nu_1 = -C_4 NbC_1 \exp(-NbC_1) - \frac{S_0}{NbC_1} \tag{25}$$

$$Sh_0 = 2\left[1 + \frac{Nt}{Nb}\right] - Nu_0 \tag{26}$$

$$Sh_1 = 2\left[1 + \frac{Nt}{Nb}\right] - Nu_1 \tag{27}$$

where $C_1, C_2, C_3, C_4, C_5, C_6$ are constants defined by

$$C_1 = 2\left(1 + \frac{Nt}{Nb}\right),\ C_2 = -\left(1 + \frac{Nt}{Nb}\right),\ C_3 = \frac{\left[(NbC_1)^2(1+\exp(-NbC_1)) + S_0(\exp(-NbC_1)-1) + NbC_1 S_0\right]}{NbC_1(1-\exp(-NbC_1))},$$

$$C_4 = \frac{2NbC_1 + S_0}{NbC_1(\exp(-NbC_1)-1)},\ C_5 = E_3 + \frac{dP}{dX}E_4 + \frac{Gr}{Re}E_5,\ C_6 = \left[\frac{NrNt}{Nb} + \frac{Gr}{Re}\right]\frac{C_4}{(NbC_1)^2} \tag{28}$$

Another important analysis in the study of mixed convection flow in the calculation of critical value of mixed convection parameter $\left(\frac{Gr}{Re}\right)$ The occurrence of flow reversal at the walls is found for $\frac{Gr}{Re}$ from the turning point of fluid velocity as:

$$\left.\frac{Gr}{Re}\right|_{Y=0} = \frac{E_{12}}{E_{11}} \quad \text{and} \quad \left.\frac{Gr}{Re}\right|_{Y=0} = \frac{E_{14}}{E_{13}} \tag{29}$$

where $E_{i's}$ are constants defined in appendix.

Case II: Temperature dependent heat source or sink (TDHSS)

This case uses the well-known model presented by Foraboschi and Federico to capture the temperature dependent heat source/sink as [33]:

$$Q = Q_0(T - T_0) \tag{30}$$

Incorporating equation (30) into (2-4) and using (11), the dimensionless equations governing this case are given as:

$$\frac{d^2U}{dY^2} = -\frac{dP}{dX} + Nr\phi - \frac{Gr}{Re}\theta \tag{31}$$

$$\frac{d^2\theta}{dY^2} + Nb\frac{d\theta}{dY}\frac{d\phi}{dY} + Nt\left(\frac{d\theta}{dY}\right)^2 + S\theta = 0 \tag{32}$$

$$\frac{d^2\phi}{dY^2} + \frac{Nt}{Nb}\frac{d^2\theta}{dY^2} = 0 \tag{33}$$

The solution to equations (31-33) with boundary conditions (15) and (16) is given by:

$$U(Y) = -\frac{dP}{dX}\frac{Y^2}{2} + Nr\left[\frac{C_1 Y^3}{6} + \frac{C_2 Y^2}{2}\right] - \left[\frac{NrNt}{Nb} + \frac{Gr}{Re}\right]\left[\frac{C_7 \exp(\lambda_1 Y)}{(\lambda_1)^2} + \frac{C_8 \exp(\lambda_2 Y)}{(\lambda_2)^2}\right] + C_9 Y + C_{10}$$

(34)

$$\theta(Y) = \frac{[1+\exp(\lambda_1)]\exp(\lambda_2 Y) - [1+\exp(\lambda_2)]\exp(\lambda_1 Y)}{exp(\lambda_2) - exp(\lambda_1)} \tag{35}$$

$$\phi(Y) = (2Y-1)\left[1 + \frac{Nt}{Nb}\right] - \frac{Nt}{Nb}\theta(Y) \tag{36}$$

$$\frac{dP}{dX} = Z_9 + Z_{10}\frac{Gr}{Re} \tag{37}$$

where $C_{i's}$ and λ_1, λ_2 are constants defined in appendix.

In similar manner, the skin-friction, Nusselt number and Sherwood number are obtained by the use of equation (21) on as [34-36]:

$$\tau_0 = \left[\frac{NrNt}{Nb} + \frac{Gr}{Re}\right]\left[\frac{C_7}{\lambda_1} + \frac{C_8}{\lambda_2}\right] + C_9 \tag{38}$$

$$\tau_1 = -\frac{dP}{dX} + Nr\left[\frac{C_1}{2} + C_2\right] - \left[\frac{NrNt}{Nb} + \frac{Gr}{Re}\right]\left[\frac{C_7 \exp(\lambda_1)}{\lambda_1} + \frac{C_8 \exp(\lambda_2)}{\lambda_2}\right] + C_9 \tag{39}$$

$$Nu_0 = \frac{\lambda_2[1+\exp(\lambda_1)] - \lambda_1[1+\exp(\lambda_2)]}{exp(\lambda_2) - exp(\lambda_1)} \tag{40}$$

$$Nu_1 \frac{\lambda_2[1+\exp(\lambda_1)]\exp(\lambda_2) - \lambda_1[1+\exp(\lambda_2)]\exp(\lambda_1)}{exp(\lambda_2) - exp(\lambda_1)} \tag{41}$$

$$Sh_0 = 2\left[1 + \frac{Nt}{Nb}\right] - Nu_0 \tag{42}$$

$$Sh_1 = 2\left[1 + \frac{Nt}{Nb}\right] - Nu_1 \tag{43}$$

$$\left.\frac{Gr}{Re}\right|_{Y=0} = \frac{Z_{12}}{Z_{11}} \quad \text{and} \quad \left.\frac{Gr}{Re}\right|_{Y=0} = \frac{Z_{14}}{Z_{13}} \tag{44}$$

where $Z_{i's}$ are constants defined in appendix.

Results and Discussion

This article is devoted to analyse the role of heat generation/absorption on mixed convection flow formation in a vertical macro channel filled with nanofluid. The accuracy of the exact solutions obtained are justify by comparing the pressure gradient and skin-friction in this current research with those of Grosan and Pop [9] by relaxing the heat source/sink parameter. This comparison gives an excellent agreement.

To have a noticeable insight on flow formation, Figures 2-8 are depicted to show the role of various pertinent parameters governing the flow formation. Throughout this article, the values of the parameters are used exactly with those of [9] for easy verification of results. -5≤S_0=S≤5, the Brownian motion parameter (Nb), thermophoresis parameter (Nt) and buoyancy-ratio parameter (Nr) are selcected as: 0≤Nb=Nt≤0.5,0≤Nr≤1000,0≤Gr/Re≤1000. It is good to state that positive values of S_0 and S signify heat source while negative values signifies heat sink.

(Figure 2) presents temperature distributions for constant heat source/sink (CHSS) and temperature dependent heat source/sink cases (TDHSS) for different values of source/sink parameter. It is obvious that for both cases, fluid temperature increases with increase in . This is so because positive values of signify addition of heat to fluid flow which in turns leads to enhancement of temperature distribution. Another obvious is that temperature is higher in the case of CHSS than TDHSS. This could be physically attributed to the fact that there exists uniform heat source throughout the channel for the case of CHSS and hence exhibits higher temperature distributions than the case of TDHSS.

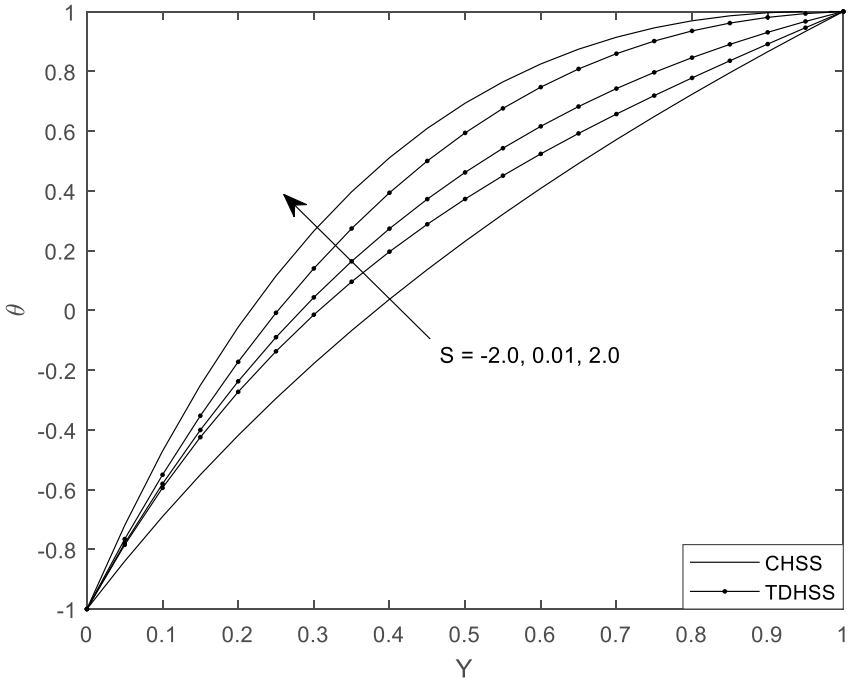

Figure 2: Temperature profiles for different values of S at Nb=0.5

(Figure 3) on the other hand depicts the rescaled nanoparticle volume fraction for different values of S . It is found that nanoparticle volume fraction decreases with increase in heat source/sink parameter and the maximum volume fraction is observed for the case of CHSS.

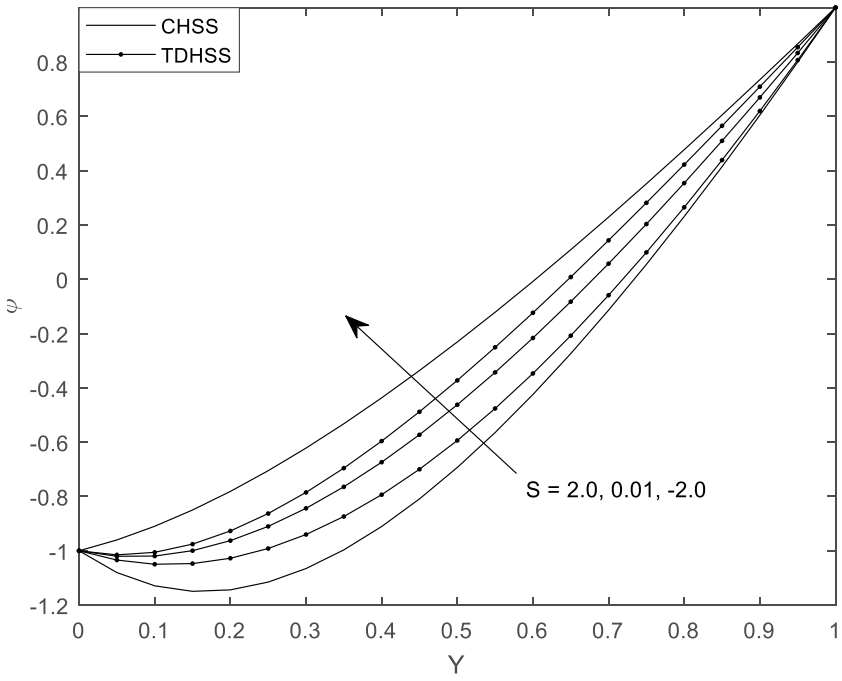

Figure 3: Nanoparticle volume fraction for different values of S at Nb=0.5 ,Nt=0.5

(Figs. 4a and 4b) illustrate the role of buoyancy-ratio parameter (*Nr*) on fluid velocity for the case of CHSS and TDHSS respectively. It is noticed for both cases that the role of *Nr* is to decrease fluid velocity at the cooled wall and otherwise at the heated wall. It is good to also state that increase in *Nr* leads to increase in region with flow reversal at the cooled wall. This could be attributed to the fact that *Nr* is sufficient in inducing reverse flow at the channel walls, hence, the increase in magnitude of leads to enhancement of region of flow reversal. Also, there is occurrence of flow reversal at the heated wall in the absence of *Nr*. This is true since the occurrence of reverse flow is strictly initiated by mixed convection parameter in clear fluid.

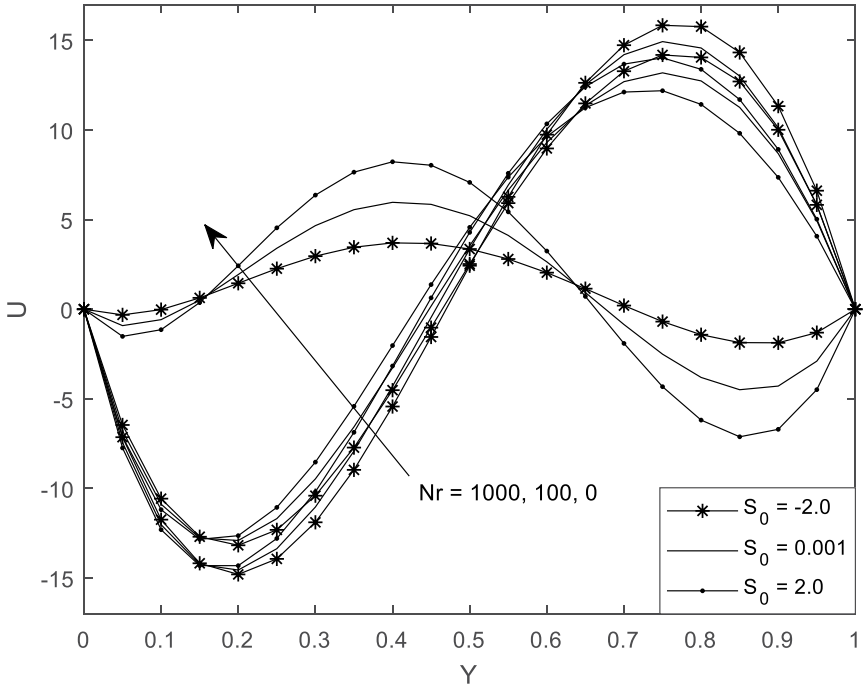

Figure 4a: Velocity profile for different values of S_0 and Nr at Nb=0.5 ,Nt=0.5, Gr/Re=1000

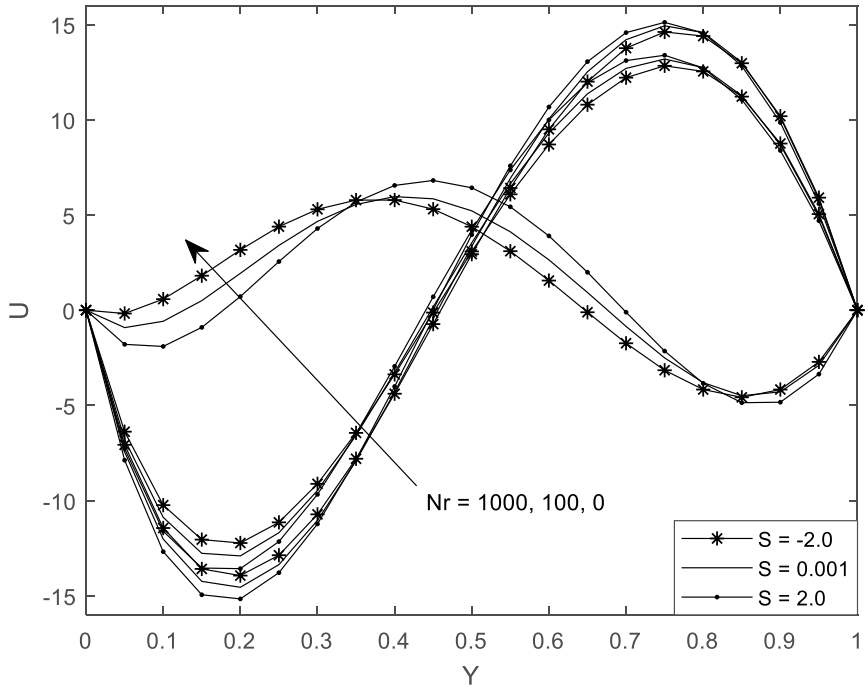

Figure 4b: Velocity profile for different values of S and Nr at Nb=0.5 ,Nt=0.5, Gr/Re=1000

(Figure 5) shows a graphical comparison on the role of heat source of fluid velocity for different physical situations. Two points of intersection are observed between the clear fluid and the heat generating ones. These inflexion points are strictly dependent on the case considered. It is noticed that fluid velocity is highest for the case of clear fluid towards the walls than those of heat source/sink cases while the reverse situation occurs around the centre of the channel.

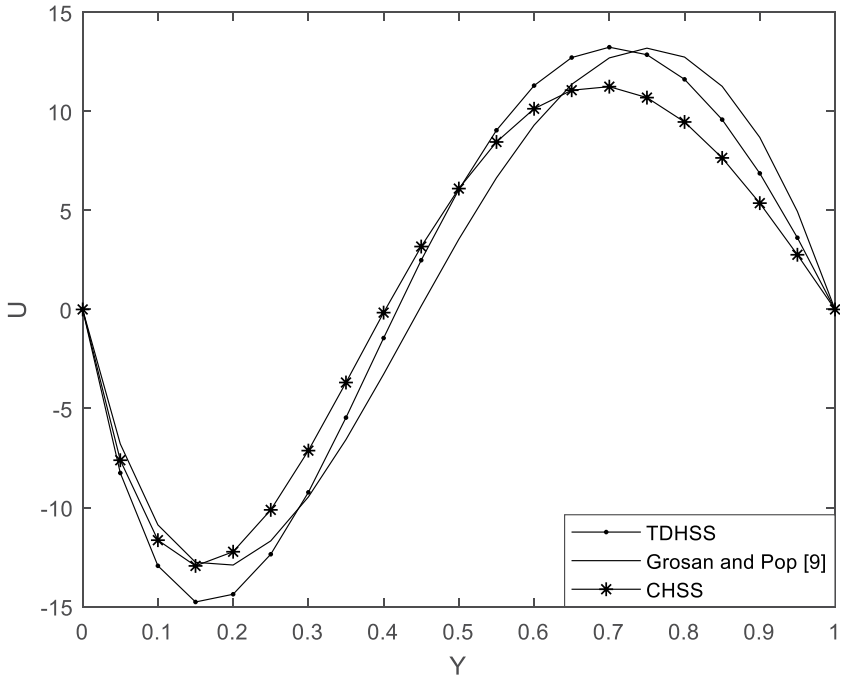

Figure 5: Velocity profile for different physical cases at S_0=S=5.0,Nb=0.5 ,Nt=0.5,Nr=100, Gr/Re=1000

(Figure 6) presents the rate of heat transfer (represented by Nusselt number) at the cooled surface for different values of *Nt* and heat source/sink parameter. It is obvious from this figure that heat transfer decreases with increase in *Nt* but increases for heat source and decreases for heat sink. In addition, the maximum heat transfer at the cooled wall is observe for the case of CHSS. This can be attributed to the increase in temperature difference between the cooled wall and the constantly applied heat source/sink fluid, therefore increasing the Nusselt number.

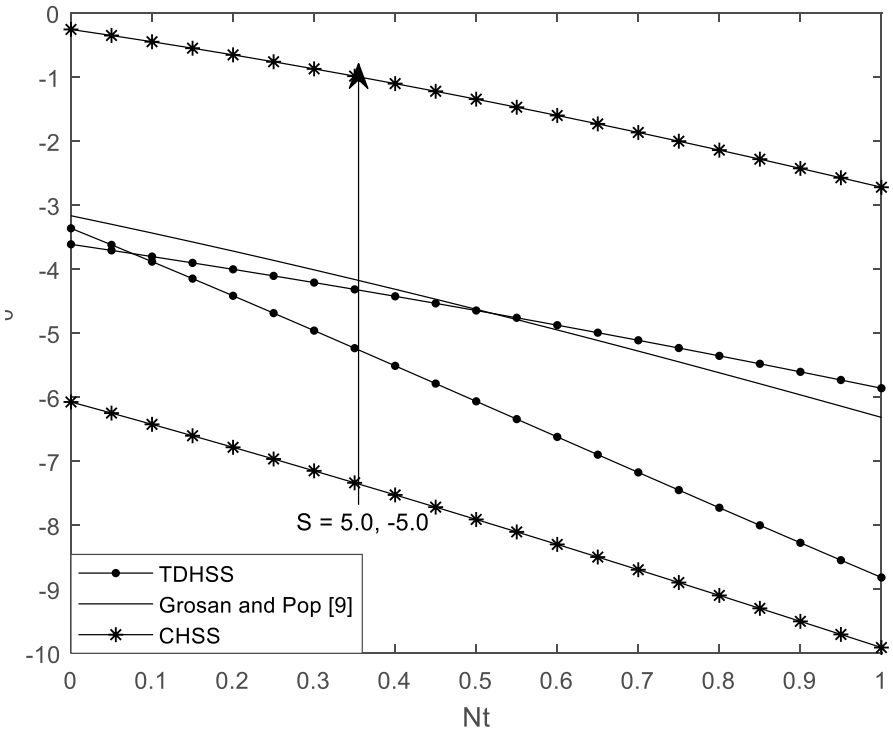

Figure 6: Nusselt number for different physical cases and varying values of Nt at Nb=0.5

(Figure 7) on the other hand depicts the combined effects of heat source/sink and thermophoresis parameter on Sherwood number. It is evident that *Sh* increases with increase in *Nt*. Also, heat sink situation gives a higher value of *Sh*. This can be explained by that thermophoresis parameter increases the ratio of convective mass transfer to mass diffusion rate and therefore enhancing the Sherwood number. In similar way, (Figure 8) gives the skin-friction between the fluid and the cooled wall for different values of heat source/sink parameter, *Nt* and different physical situations. It is seen that the drag force increases with increase in *Nt* and heat source regardless of the physical situation considered. Also, skin-friction at this cooled wall is observed to be higher for the case of CHSS compared to the TDHSS case. This is as a result of corresponding increase noticed in dimensionless velocity with respect to heat source, hence increases the force at which the fluid hits the surface of the cooled channel.

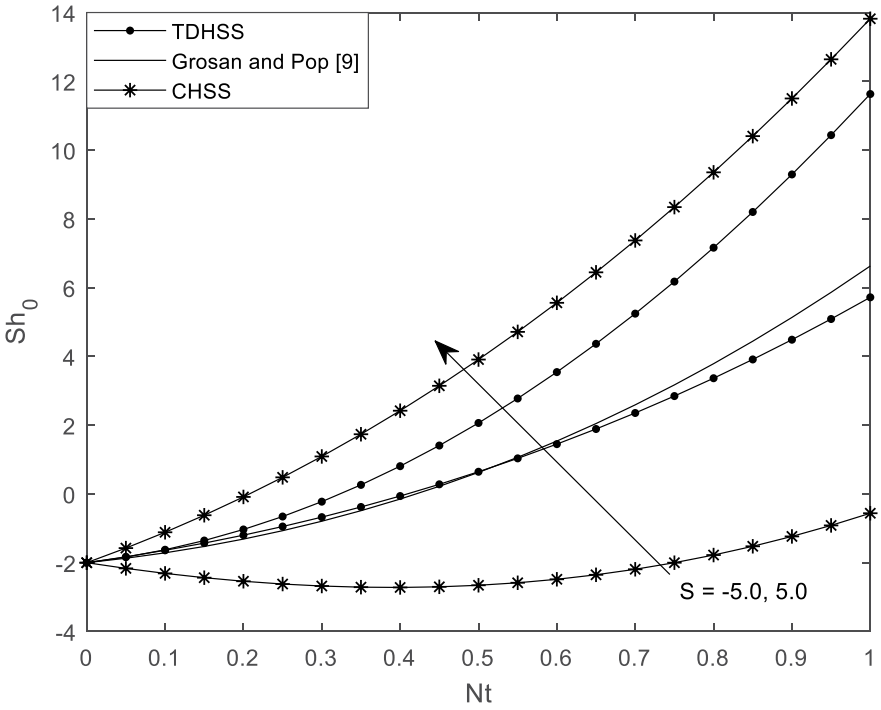

Figure 7: Sherwood number for different physical cases and varying values of Nt at Nb=0.5

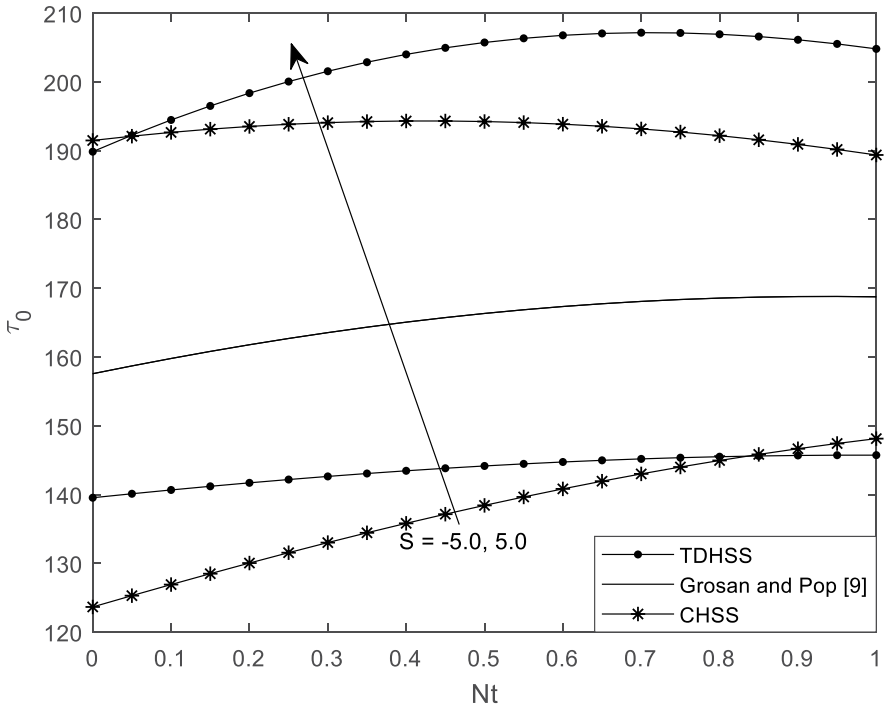

Figure 8: Skin-friction for different physical cases and varying values of Nt at Nb=0.5,Nr=100, Gr/Re=1000

For test of accuracy,

Table 1 provides numerical comparisons of present work pressure gradient and skin-friction as $S = S_0 \rightarrow 0$ with those of [36]. It is obvious that this comparison gives excellent agreement. Table 2 on the hand exhibits the degree of dependency of heat source/sink parameter on Nusselt number, Sherwood number and skin-friction for fixed value of other parameters. (S_{lp}) This rate of increase or decrease of relevant profiles due to the increase in heat source/sink parameter is estimated using slope of the linear regression line through data points in known dependent and independent variables [26, 27]. From Table 3, it is obvious that Nusselt number, Sherwood number and skin-friction respond to change in heat source/sink parameter for the case of TDHSS than CHSS. This can be credited to the varying nature of the TDHSS case with temperature and hence responds more to change in magnitude of heat source/sink parameter.

Table 1: Numerical comparisons of pressure gradient and skin-friction with those of Grosan and Pop [9]

$\frac{Gr}{Re}$	Nr	Nt	Nb	α			τ_0		
				Grosan and Pop [9]	Case I ($S_0 = 0$)	Case II ($S \rightarrow 0$)	Grosan and Pop [9]	Case I ($S_0 = 0$)	Case II ($S \rightarrow 0$)
0	0.0	0.0	0.2	12.000	12.000	12.000	-6.0000	-6.0000	-6.0000
	0.0	0.2	0.2	12.000	12.000	12.000	-6.0000	-6.0000	-6.0000
	5.0	0.2	0.2	11.2090	11.2090	11.2090	-6.7764	-6.7764	-6.7764
1000	0.0	0.0	0.2	-67.7723	-67.7723	-67.7723	166.8653	166.8653	166.8653
	0.0	0.2	0.2	-146.1992	-146.1992	-146.1992	172.0489	172.0489	172.0489
	5.0	0.2	0.2	-146.9902	-146.9902	-146.9902	171.2725	171.2725	171.2725

Table 2: Numerical computation of Nusselt number, Sherwood number and skin-friction at Nt=Nb=0.5,Nr=100,Gr/Re=1000,Y=1.0

S	Nu_1		Sh_1		τ_1	
	Case I	Case II	Case I	Case II	Case I	Case II
0.0001	0.6261	0.6260	3.3739	3.3740	-111.3443	-111.3443
2.0	-0.0609	0.0793	4.0609	3.9207	-89.0164	-103.7072
3.0	-0.4044	-0.2500	4.4044	4.2500	-77.8525	-97.3486
5.0	-1.0913	-1.1062	5.0913	5.1062	-55.5247	-74.8476
10.0	-2.8088	-14.2252	6.8088	18.2252	0.2950	-594.7974
Slp	**-0.3435**	**-1.5323**	**0.3455**	**1.5323**	**11.1639**	**73.3824**

Table 3: Numerical computations for critical values of Gr/Re for different values of S and Nr at Nt=Nb=0.5

S	Nr	CHSS		TDHSS	
		$\frac{Gr}{Re}\Big\|_{Y=0}$	$\frac{Gr}{Re}\Big\|_{Y=1}$	$\frac{Gr}{Re}\Big\|_{Y=0}$	$\frac{Gr}{Re}\Big\|_{Y=1}$
	0.0	37.1305	-33.9336	35.9702	-45.8035
	10	47.7586	-25.0816	45.9537	-30.3571
-5.0	100	143.4112	54.5866	135.8047	108.6605
	1000	1099.90	851.2686	1034.30	1498.80
0.001	0.0	32.0916	-47.5924	32.0916	-47.5924
	10	39.9203	-31.1522	39.9203	-31.1522
	100	110.3784	116.8098	110.3784	116.8098
	1000	814.9592	1596.40	814.9592	1596.40
	0.0	28.2569	-79.6544	26.9317	-64.5913
	10	33.9552	-45.4019	31.8938	-38.7072
5.0	100	85.2399	262.8698	76.5525	194.2493
	1000	598.0865	3345.60	523.1395	2523.80

Conclusion

The present article analysed the role of constantly applied heat source/sink or temperature dependent heat source/sink on mixed convection flow in a vertical channel filled with nanofluid. Based on the exact solutions and depicted graphs obtained for flow formation in the vertical channel, the following conclusions can be drawn:

1. Temperature, nanoparticle volume fraction, Nusselt number and Sherwood number is higher in the case of CHSS than TDHSS
2. TDHSS responds faster to change in heat source parameter than the CHSS
3. The impact of buoyancy distribution parameter is to increase reverse flow at the cooled wall
4. The interval of no reverse flow can be increased by increasing the magnitude of heat source/sink parameter.

The findings obtained in this current article have important implication in engineering applications and optimization of backward flow by careful selection of governing parameters.

COI On behalf of all authors, the corresponding author states that there is no conflict of interest.

References

1. Tao, L. N. (1960). On combined free and forced convection in channels, 82:233-238.
2. Beckett, P. M. (1980). Combined natural-and forced-convection between parallel vertical walls. SIAM Journal on Applied Mathematics, 39(2), 372-384.
3. Aung, W., & Work, G. (1986). Theory of fully developed, combined convection including flow reversal, 23:485-488.
4. Oztop, H. F., & Abu-Nada, E. (2008). Numerical study of natural convection in partially heated rectangular enclosures filled with nanofluids. International journal of heat and fluid flow, 29(5), 1326-1336.
5. Choi, S. U., & Eastman, J. A. (1995). Enhancing thermal conductivity of fluids with nanoparticles (No. ANL/MSD/CP-84938; CONF-951135-29). Argonne National Lab. (ANL), Argonne, IL (United States), Vol. 66:99-105.
6. Wong, K. V., & De Leon, O. (2010). Applications of nanofluids: current and future. Advances in mechanical engineering, 2, 519659.
7. Buongiorno, J. (2006). Convective transport in nanofluids, 128:240-250.
8. Nield, D. A., & Kuznetsov, A. V. (2009). The Cheng–Minkowycz problem for natural convective boundary-layer flow in a porous medium saturated by a nanofluid. International Journal of Heat and Mass Transfer, 52(25-26), 5792-5795.
9. Grosan, T., & Pop, I. (2012). Fully developed mixed convection in a vertical channel filled by a nanofluid. Journal of heat transfer, 134:82501-82505.
10. Kuznetsov, A. V., & Nield, D. A. (2010). Natural convective boundary-layer flow of a nanofluid past a vertical plate. International Journal of Thermal Sciences, 49(2), 243-247.
11. Khan, W. A., & Pop, I. (2010). Boundary-layer flow of a nanofluid past a stretching sheet. International journal of heat and mass transfer, 53(11-12), 2477-2483.

12. Kang, H. U., Kim, S. H., & Oh, J. M. (2006). Estimation of thermal conductivity of nanofluid using experimental effective particle volume. Experimental Heat Transfer, 19(3), 181-191.
13. Khanafer, K., Vafai, K., & Lightstone, M. (2003). Buoyancy-driven heat transfer enhancement in a two-dimensional enclosure utilizing nanofluids. International journal of heat and mass transfer, 46(19), 3639-3653.
14. Aminossadati, S. M., & Ghasemi, B. (2009). Natural convection cooling of a localised heat source at the bottom of a nanofluid-filled enclosure. European Journal of Mechanics-B/Fluids, 28(5), 630-640.
15. Inman, R. M. (1962). Experimental study of temperature distribution in laminar tube flow of a fluid with internal heat generation. International Journal of Heat and Mass Transfer, 5(11), 1053-1058.
16. Ostrach, S. (1954). Combined natural-and forced-convection laminar flow and heat transfer of fluids with and without heat sources in channels with linearly varying wall temperatures. NATIONAL AERONAUTICS AND SPACE ADMINISTRATION CLEVELAND OH GLENN RESEARCH CENTER., NACA TN, 3141.
17. Chambré, P. L. (1957). The laminar boundary layer with distributed heat sources or sinks*. Applied Scientific Research, Section A, 6(5), 393-401.
18. Toor, H. L. (1958). Heat transfer in forced convection with internal heat generation. AIChE Journal, 4(3), 319-323.
19. Moalem, D. (1976). Steady state heat transfer within porous medium with temperature dependent heat generation. International Journal of Heat and Mass Transfer, 19(5), 529-537.
20. Foraboschi, F. P., & Di Federico, I. (1964). Heat transfer in laminar flow of non-Newtonian heat-generating fluids. International Journal of Heat and Mass Transfer, 7(3), 315-325.
21. Sparrow, E. M., Chrysler, G. M., & Azevedo, L. F. (1984). Observed flow reversals and measured-predicted Nusselt numbers for natural convection in a one-sided heated vertical channel, 106,(2), 325-332.
22. Aung, W., & Work, G. (1986). Developing flow and flow reversal in a vertical channel with asymmetric wall temperatures, 108, 485-488.
23. Jha, B. K., & Oni, M. O. (2018). Mixed convection flow in a vertical channel with temperature dependent viscosity and flow reversal: An exact solution. Journal homepage: http://iieta. org/Journals/IJHT, 36(2), 607-613.
24. Oni, M. O. (2017). Combined effect of heat source, porosity and thermal radiation on mixed convection flow in a vertical annulus: An exact solution. Engineering Science and Technology, an International Journal, 20(2), 518-527.
25. Jha, B. K., Oni, M. O., & Aina, B. (2018). Steady fully developed mixed convection flow in a vertical micro-concentric-annulus with heat generating/absorbing fluid: an exact solution. Ain Shams Engineering Journal, 9(4), 1289-1301,
26. Animasaun, I. L., & Pop, I. (2017). Numerical exploration of a non-Newtonian Carreau fluid flow driven by catalytic surface reactions on an upper horizontal surface of a paraboloid of revolution, buoyancy and stretching at the free stream. Alexandria Engineering Journal, 56(4), 647-658,
27. Shah, N. A., Animasaun, I. L., Ibraheem, R. O., Babatunde, H. A., Sandeep, N., & Pop, I. (2018). Scrutinization of the effects of Grashof number on the flow of different fluids driven by convection over various surfaces. Journal of Molecular liquids, 249, 980-990.

Appendix I (Case I)

$$E_1 = Nr\frac{Nt}{Nb}\frac{C_4}{(NbC_1)^2}, E_2 = \frac{C_4}{(NbC_1)^2}, \quad E_3 = Nr\frac{Nt}{Nb}\left[\frac{S_0}{2(NbC_1)^2} - \frac{S_0}{6NbC_1} + \frac{C_3}{2NbC_1} + \frac{C_4 exp\,(-NbC_1)}{(NbC_1)^2}\right] -$$

$$Nr\left[\frac{C_1}{6} + \frac{C_2}{2}\right] - E_1, E_4 = \frac{1}{2}, \quad E_5 = \left[\frac{S_0}{2(NbC_1)^2} - \frac{S_0}{6NbC_1} + \frac{C_3}{2NbC_1} + \frac{C_4 exp\,(-NbC_1)}{(NbC_1)^2}\right] - E_2, \quad E_6 = \frac{1}{6} -$$

$$\frac{E_4}{2}, \quad E_7 = Nr\left[\frac{C_1}{24} + \frac{C_2}{6}\right] - Nr\frac{Nt}{Nb}\left[\frac{S_0}{6(NbC_1)^2} - \frac{S_0}{24NbC_1} + \frac{C_3}{6NbC_1} - \frac{C_4(exp\,(-NbC_1)-1)}{(NbC_1)^3}\right] + \frac{E_3}{2} + E_1 -$$

$$1, \quad E_8 = \frac{E_5}{2} + \frac{E_2}{2} - \frac{S_0}{6(NbC_1)^2} + \frac{S_0}{24NbC_1} - \frac{C_3}{6NbC_1} + \frac{C_4(exp\,(-NbC_1)-1)}{(NbC_1)^3}, \quad E_9 = \frac{E_7}{E_6}, \quad E_{10} = \frac{E_8}{E_6},$$

$$E_{11} = \frac{C_3}{NbC_1} + E_5 + E_4E_{10}, \quad E_{12} = -Nr\frac{Nt}{Nb}\frac{C_3}{NbC_1} - E_3 - E_4E_9, \quad E_{13} = E_{10} - E_4E_{10} - E_5 +$$

$$\left[\frac{S_0}{(NbC_1)^2} - \frac{S_0}{2NbC_1} + \frac{C_3}{NbC_1} - \frac{C_4 exp\,(-NbC_1)}{NbC_1}\right], \quad E_{14} = E_3 + E_4E_{10} + Nr\left[\frac{C_1}{2} + C_2\right] - E_9 -$$

$$Nr\frac{Nt}{Nb}\left[\frac{S_0}{(NbC_1)^2} - \frac{S_0}{2NbC_1} + \frac{C_3}{NbC_1} - \frac{C_4 exp\,(-NbC_1)}{NbC_1}\right]$$

Appendix II (Case II)

$$C_7 = -\frac{[\exp(\lambda_2)+1]}{\exp(\lambda_2)-\exp(\lambda_1)}, C_8 = \frac{[\exp(\lambda_2)+1]}{\exp(\lambda_2)-\exp(\lambda_1)} \quad , \quad \lambda_1 = \frac{1}{2}\left[-NbC_1 + \sqrt{(NbC_1)^2 - 4S}\right],$$

$$\lambda_2 = \frac{1}{2}\left[-NbC_1 - \sqrt{(NbC_1)^2 - 4S}\right], \; C_9 = Z_1 + Z_2\frac{Gr}{Re}, \; C_{10} = Z_3 + Z_4\frac{Gr}{Re} + Z_5\frac{dP}{dX}, \; Z_1 =$$

$$Nr\frac{Nt}{Nb}\left[\frac{C_7}{\lambda_1^2} + \frac{C_8}{\lambda_2^2}\right], \; Z_2 = \left[\frac{C_7}{\lambda_1^2} + \frac{C_8}{\lambda_2^2}\right], \; Z_3 = Nr\frac{Nt}{Nb}\left[\frac{C_7\exp(\lambda_1)}{\lambda_1^2} + \frac{C_8\exp(\lambda_2)}{\lambda_2^2}\right] - Z_1 - Nr\left[\frac{C_1}{6} + \frac{C_2}{2}\right],$$

$$Z_4 = \left[\frac{C_7\exp(\lambda_1)}{\lambda_1^2} + \frac{C_8\exp(\lambda_2)}{\lambda_2^2}\right] - Z_2, \; Z_5 = \frac{1}{2}, \quad Z_6 = \frac{1}{6} - \frac{Z_5}{2}, Z_7 = Nr\left[\frac{C_1}{24} + \frac{C_2}{6}\right] -$$

$$Nr\frac{Nt}{Nb}\left[\frac{C_7(\exp(\lambda_1)-1)}{\lambda_1^3} + \frac{C_8(\exp(\lambda_2)-1)}{\lambda_2^3}\right] + Z_1 + \frac{Z_3}{2} - 1, Z_8 = Z_2 + \frac{Z_4}{2} - \left[\frac{C_7(\exp(\lambda_1)-1)}{\lambda_1^3} +\right.$$

$$\left.\frac{C_8(\exp(\lambda_2)-1)}{\lambda_2^3}\right], Z_9 = \frac{Z_7}{Z_6}, \; Z_{10} = \frac{Z_8}{Z_6}, \; Z_{11} = \left[\frac{C_7}{\lambda_1} + \frac{C_8}{\lambda_2}\right] - Z_4 - Z_5Z_{10}, \; Z_{12} = Z_3 + Z_5Z_9 -$$

$$Nr\frac{Nt}{Nb}\left[\frac{C_7}{\lambda_1} + \frac{C_8}{\lambda_2}\right], \quad Z_{13} = Z_{10} - Z_4 - Z_5Z_{10} + \left[\frac{C_7\exp(\lambda_1)}{\lambda_1} + \frac{C_8\exp(\lambda_2)}{\lambda_2}\right], \quad Z_{14} = Nr\left[\frac{C_1}{2} + C_2\right]$$

$$Z_9 + Z_3 + Z_5Z_9 - Nr\frac{Nt}{Nb}\left[\frac{C_7\exp(\lambda_1)}{\lambda_1} + \frac{C_8\exp(\lambda_2)}{\lambda_2}\right]$$